Research Article Vol. 38, No. 4 / April 2021 / Journal of the Optical Society of America B 1325

Journal of the Optical Society of America B

OPTICAL PHYSICS

Engineering light absorption at critical coupling via bound states in the continuum

Shuyuan Xiao,[1,2,5] Xing Wang,[1,2] Junyi Duan,[1,2] Tingting Liu,[3,6] and Tianbao Yu[4,7]

[1]Institute for Advanced Study, Nanchang University, Nanchang 330031, China
[2]Jiangxi Key Laboratory for Microscale Interdisciplinary Study, Nanchang University, Nanchang 330031, China
[3]School of Physics and Electronics Information, Hubei University of Education, Wuhan 430205, China
[4]Department of Physics, Nanchang University, Nanchang 330031, China
[5]e-mail: syxiao@ncu.edu.cn
[6]e-mail: ttliu@hue.edu.cn
[7]e-mail: yutianbao@ncu.edu.cn

Received 5 January 2021; revised 17 February 2021; accepted 3 March 2021; posted 3 March 2021 (Doc. ID 419191); published 24 March 2021

Recent progress in nanophotonics is driven by the desire to engineer light–matter interaction in two-dimensional (2D) materials using high-quality resonances in plasmonic and dielectric structures. Here, we demonstrate a link between radiation control at critical coupling and metasurface-based bound states in the continuum (BIC) physics, and develop a generalized theory to engineer light absorption of 2D materials in coupling resonance metasurfaces. In a typical example of hybrid graphene–dielectric metasurfaces, we present manipulation of the absorption bandwidth by more than one order of magnitude by simultaneously adjusting the asymmetry parameter of silicon resonators governed by BIC and graphene surface conductivity while the absorption efficiency remains maximum. This work reveals the generalized role of BIC in radiation control at critical coupling, and provides promising strategies in engineering light absorption of 2D materials for high-efficiency optoelectronics device applications, e.g., light emission, detection, and modulation.

https://doi.org/10.1364/JOSAB.419191

1. INTRODUCTION

Over the past decade, two-dimensional (2D) materials have emerged as promising core elements in next-generation optoelectronic devices due to their exceptional optical and electric properties [1]. The main obstacle to practical applications is the relatively weak light–matter interaction, and it is of paramount importance to enhance light absorption in these atomically thin films. J. R. Piper introduced a concept of critical coupling to engineer light absorption with a photonic crystal guided resonance. The absorption in the top graphene can reach maximum when the external radiation rate of the guided resonance equals the internal dissipative loss rate of graphene [2,3]. Such a system shows great advantages over a Fabry–Perot cavity in simplicity of fabrication, robust performance, and compatible features, and has inspired exploration of absorption in the whole family of 2D materials [4–21].

In the above-mentioned critical coupling systems, several key figures of the absorption properties including central location, efficiency, and bandwidth can be tuned by adjusting the geometric parameters of photonic crystal slabs. The absorption engineering essentially originates from control of the radiation rate of the guided resonance. In reality, this kind of radiation control based on the dependence of geometrical parameters is ubiquitous in the field of nanophotonics, which is definitely not limited to the guided resonance in photonic crystal slabs [22–24], but also universally applicable to resonance modes in a variety of seemingly different photonic structures such as trapped modes [25–30], toroidal modes [31–33], non-radiating anapole modes [34–37], and supercavity modes [38,39], which are fundamentally linked to the physics of bound states in the continuum (BIC).

In this work, we demonstrate a link between radiation control at critical coupling and fascinating BIC physics, and develop a general theory to engineer light absorption of 2D materials in coupling resonance metasurfaces. As an example, we place monolayer graphene on top of asymmetric pairs of silicon nanobars. The maximum absorption of graphene is attained under the critical coupling condition when the radiation rate of the trapped mode in the resonators is equal to the dissipative loss of graphene. By simultaneously adjusting the asymmetry parameter for the resonators and the graphene surface conductivity, the absorption bandwidth can be flexibly tuned in good agreement with theoretical predictions while the absorption efficiency remains maximum. This work reveals the generalized role of BIC in radiation control at critical coupling, and delineates an

in-depth conceptual framework and novel promising strategies in engineering light absorption of 2D materials for smart design of compact optoelectronic devices.

2. THEORETICAL FORMALISM

The coupled mode theory (CMT) is utilized to provide insight into the input and output properties of a resonance system. We consider the behavior of a mirror-symmetric resonator that possesses a single resonance mode coupling with outside circumstances via two identical ports. For a lossless system, the dynamic equations can be written as [40,41]

$$\frac{da}{dt} = (i\omega_0 - \gamma)a + D^T|s_+\rangle, \tag{1}$$

$$|s_-\rangle = C|s_+\rangle + Da, \tag{2}$$

where a is the resonance amplitude, ω_0 and γ represent the resonance frequency and radiation rate, respectively, $|s_+\rangle = [s_{1+}, s_{2+}]^T$, $|s_-\rangle = [s_{1-}, s_{2-}]^T$, and $D = [d_1, d_2]^T$ represent the input waves, output wave, and coupling matrix, respectively, and C is the scattering matrix of the direct coupling pathway. In such a system, the resonance mode is excited by the input waves $|s_+\rangle$ from ports 1, 2 with coupling matrix D^T, and the excited resonance mode couples with the output waves $|s_-\rangle$ at the ports with coupling matrix D. The dynamic equations are constrained by energy-conservation and time-reversal symmetry considerations. For the case where the input wave with unit amplitude is incident from only a single port, the stored energy in the resonator can be derived from the general formalism of Eqs. (1) and (2):

$$|a|^2 = \frac{\gamma}{(\omega - \omega_0)^2 + \gamma^2}. \tag{3}$$

Further, when the dissipative loss is inserted into the system and the underlying symmetry of the structure remains unchanged, the dynamic Eq. (1) can be accordingly modified by adding the effect of the dissipative loss rate δ, i.e., $da/dt = (i\omega_0 - \gamma - \delta)a + D^T|s_+\rangle$. Then $|a|^2$ in Eq. (3) is amended by replacing the term γ^2 in the denominator with $(\gamma + \delta)^2$, and the absorption in the resonance system can be expressed as

$$A = \frac{2\delta\gamma}{(\omega - \omega_0)^2 + (\gamma + \delta)^2}. \tag{4}$$

As can be seen in Eq. (4), the absorption of the resonance system will exhibit a symmetric Lorentzian lineshape, and three key paramaters, ω_0, γ, and δ, determine the absorption characteristics. More specifically, the resonance frequency ω_0 predicts the central location of the absorption spectrum, i.e., the center frequency of the Lorentzian lineshape, and the radiation rate γ and dissipative loss rate δ jointly define the efficiency and bandwidth of absorption. At the resonance frequency $\omega = \omega_0$, the absorption A_0 is determined by the ratio between γ and δ:

$$A_0 = \frac{2}{\frac{\gamma}{\delta} + \frac{\delta}{\gamma} + 2}, \tag{5}$$

which will attain a theoretical maximum of 0.5 when $\gamma = \delta$. This is the so-called critical coupling condition for a single resonance in a two-port system.

The absorption bandwidth is usually defined as the full width at half maximum (FWHM). Assuming the half maximum absorption $A_1 = A_0/2$ occurs at ω_1, $\Gamma^{\mathrm{FWHM}} = 2|\omega_1 - \omega_0|$ can be calculated as

$$\Gamma^{\mathrm{FWHM}} = 2(\gamma + \delta). \tag{6}$$

In association with the general wave phenomenon of BIC, the radiaiton rate γ of a resonance mode is considered as the mode inverse radiation lifetime. An ideal symmetry-protected BIC has no access to radiation channels and thus can be treated as a resonance with infinite lifetime and vanishing linewidth, i.e., $\gamma = 0$. Then the quasi-BICs concept is introduced in practice, which couples to the extended waves and radiates as a leaky resonance with $\gamma > 0$ when the symmetry of a resonator is broken to generate radiation channels. Formulated from analytical calculations, the radiation rate γ is calculated by the sum of radiation losses into all the radiation channels [42,43]:

$$\gamma = c\sum_{i=x,y}|D_i|^2, \tag{7}$$

with the coupling amplitudes D_i:

$$D_{x,y} = -\frac{k_0}{\sqrt{2S_0}}\left(p_{x,y} \mp \frac{1}{c}m_{y,x} + \frac{ik_0}{6}Q_{xz,yz}\right), \tag{8}$$

where k_0 is the incident wave vector in free space, S_0 is the unit cell area, and p_α, m_α, and $Q_{\alpha\beta}$ ($\alpha, \beta = x, y, z$) are the components of electric dipole, magnetic dipole, and electric quadrupole moments in the irreducible representations, respectively.

Considering a situation where the in-plane symmetry along the x axis is broken, it follows that $D_y = 0$ since the electric field components E_x and E_y are classified as even and odd functions with respect to this symmetry. Also, m_y and Q_{xz} are both equal to zero because of the symmetry $E_x(-z) = E_x(z)$. Then a simplified analytical expression can be written as

$$\gamma = \frac{k_0^2 c}{2S_0}|p_x|^2. \tag{9}$$

$p_x = \pm\alpha p_0$ is defined as the net dipole moment in an asymmetric resonator, where p_0 is the electric dipole moment in an according symmetric case, and α is the asymmetry parameter. Then for a general kind of metasurface with an asymmetric unit cell, the radiation rate γ of the quasi-BIC can be found to be dependent on the asymmetry parameter

$$\gamma = \frac{k_0^2 c}{2S_0}|p_0|^2\alpha^2. \tag{10}$$

Substituing the expression of γ in Eq. (10) into the absorption bandwidth at critical couping in Eq. (6), the direct dependence of FWHM on the asymmetry parameter α can be finally obtained:

$$\Gamma^{\mathrm{FWHM}} = \frac{2k_0^2 c}{S_0}|p_0|^2\alpha^2, \tag{11}$$

i.e., $\Gamma^{\mathrm{FWHM}} \propto \alpha^2$, following the universal rules for the asymmetric metasurfaces with high-quality resonance driven by BIC. Based on the quadratic scalability of FWHM, a simple but rigorous way to engineer light absorption at critical coupling is suggested by adjusting the asymmetry parameter for quasi-BIC resonators. Consequently, a general physical link between radiation control at critical coupling and BIC physics is theoretically established.

3. RESULTS AND DISCUSSION

We focus on one of the examples in which a common 2D material of monolayer graphene is deposited on top of a typical dielectric metasurface that supports the magnetic dipole mode, as shown in Fig. 1. The unit cell is periodically arranged with a lattice constant $P = 900$ nm, and composed of a pair of parallel, geometrically asymmetric nanobars with a fixed separation of $D = 250$ nm. The thickness and width of the nanobars are the same values of $H = 160$ nm and $W = 200$ nm, respectively, while their lengths are set with a variable L_1 and a fixed $L_2 = 750$ nm for each case investigated. In accordance with the fact that a symmetry-protected BIC can be transformed into a quasi-BIC by simply breaking the symmetry of the system, it is predictable that the quasi-BIC state can be realized by opening a radiation channel via introducing a perturbation in the nanobar pair.

Silicon is chosen as the dielectric building material because it is characterized by a high refractive index and negligible absorption loss in the studied spectral range of near infrared. For simplification, silicon is assumed to be lossless with a refractive index of $n = 3.5$. On the other hand, the monolayer graphene on the top can be considered as an ultra-thin lossy film. The optical properties of graphene can be captured by random phase approximation (RPA) in the local limit, where the surface conductivity is expressed by the sum of intraband and interband contributions [44,45]:

$$\sigma_g = \frac{2e^2 k_B T}{\pi \hbar^2} \frac{i}{\omega + i\tau^{-1}} \ln\left[2\cosh\left(\frac{E_F}{2k_B T}\right)\right] + \frac{e^2}{4\hbar}\left[\frac{1}{2} + \frac{1}{\pi}\arctan\left(\frac{\hbar\omega - 2E_F}{2k_B T}\right) - \frac{i}{2\pi}\ln\frac{(\hbar\omega + 2E_F)^2}{(\hbar\omega - 2E_F)^2 + 4(k_B T)^2}\right]. \quad (12)$$

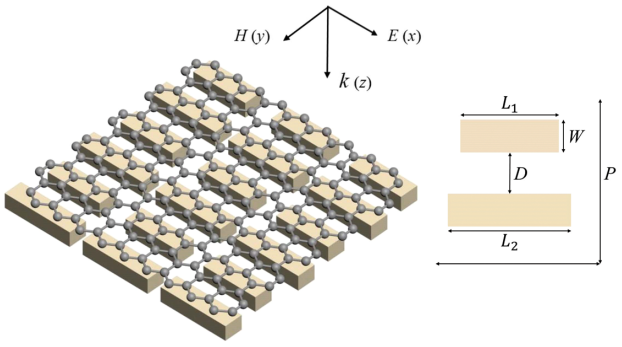

Fig. 1. Schematic of the proposed hybrid graphene–dielectric metasurfaces.

e, k_B, T, $\hbar$, and ω are the electron charge, Boltzmann constant, room temperature, reduced Planck's constant, and incident light frequency, respectively. The relaxation time τ depends on the carrier mobility μ, Fermi level E_F, and Fermi velocity v_F with the relation $\tau = (\mu E_F)/(e v_F^2)$, where the measured values $\mu = 10000$ cm^2/V·s and $v_F = 1 \times 10^6$ m/s are adopted. In particular, it is able to be controlled as the Fermi level varies. As a consequence of increasing the Fermi level, the imaginary part shows a continuous increase, and the real part reduces noticeably at the critical point of the Fermi level exceeding the Dirac point by half photon energy, i.e., $E_F > \hbar\omega/2$ due to the Pauli-blocked effect. The tunable surface conductivity of graphene enables flexible control of absorption in the resonance system. Numerical simulations are conducted using the finite-difference time-domain (FDTD) method via the Lumerical software package [46]. In the calculations, the moderate mesh grid is adopted to make a good trade-off among accuracy, memory requirements, and simulation time. The linearly polarized plane wave is incident along the $-z$ direction, the periodic boundary conditions are utilized in x and y directions, and the perfectly matching layers are adopted in the z direction. When the simulation runs, the periodic boundary conditions simply copy the electromagnetic (EM) fields that occur at one side of the simulation and inject them at the other side, therefore allowing to calculate the response of the entire structure by simulating only a unit cell.

To verify the physical picture of the radiation control at critical coupling via BIC, we first perform the resonance mode analysis without the presence of graphene. The lengths of the nanobars are set at $L_1 = 600$ nm and $L_2 = 750$ nm. Due to the in-plane symmetry breaking of the unit cell, the BIC mode manifests itself in the transmission spectrum as a Fano resonance. As shown in Fig. 2(a), the periodic dielectric structure shows a pronounced asymmetric resonance with a narrow dip at 1417.99 nm, which is well fitted by the classical Fano formula within the CMT framework [22]. The radiation rate is extracted as $\gamma = 5.99$ THz, while the dissipative loss rate is zero due to the lossless silicon nanobars here. Furthermore, the far-field radiation and near-field distribution are calculated to identify the resonance mode origin. The contributions of multipole moments to the far-field radiation are decomposed under the Cartesian coordinate system. As shown in Fig. 2(b), the dominant contribution at resonance is provided by the magnetic dipole. Here it radiates stronger than the electric quadrupole by a factor of ~4, and stronger than the radiating component of the electric dipole, magnetic quadrupole, and toroidal dipole by several orders of magnitude. The local distributions of electric, magnetic field, and displacement current are in strict accordance with this. In Figs. 2(c) and 2(d), the nanobars in the unit cell displays a magnetic dipole mode, where an anti-phase and almost equal amplitude electric polarizations are observed inside the silicon nanobars, and the circulating displacement currents in the nanobars give rise to out-of-plane magnetic dipole moments. The field profiles reveal the quasi-BIC magnetic dipole nature of the proposed metasurfaces with a highly confined EM field inside the nanobars, and this trapped mode offers a platform to engineer light–matter interactions.

Since the quasi-BIC mode is involved with the external radiation channels, the radiation rate and thus the resonance

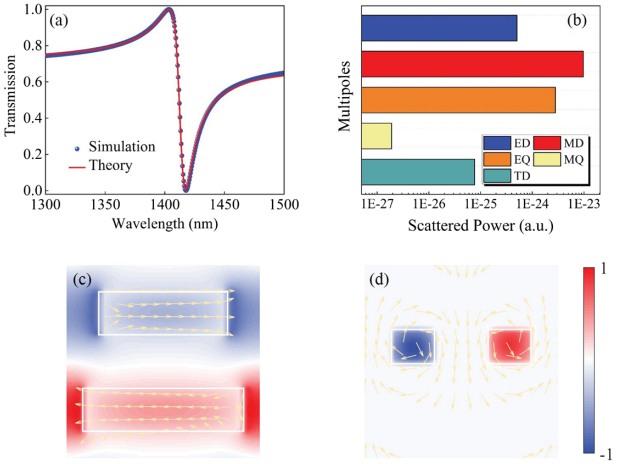

Fig. 2. (a) Simulated and fitted transmission spectra of the dielectric metasurfaces. (b) Contributions of multipole moments, including the electric dipole (ED), magnetic dipole (MD), electric quadrupole (EQ), magnetic quadrupole (MQ), and toroidal dipole (TD) to the far-field radiation of the trapped mode under Cartesian coordinates. (c) Magnitude of the x component of electric field across the unit cell at resonance wavelength, overlaid with arrows indicating direction of displacement current. (d) Corresponding magnitude of the x component of displacement current, overlaid with arrows indicating direction of magnetic field.

width can be flexibly controlled through manipulating the asymmetry degree. In the proposed dielectric metasurfaces, we observe that transmission spectra show a reducing bandwidth as the length of the shorter nanobar L_1 approaches that of the longer nanobar L_2 in Fig. 3(a), which can be attributed to a decrease in the radiation rate γ of the dielectric metasurface arising from the reduced asymmetry during the period. For a quantitative description, the asymmetry parameter α here is defined as the ratio of the reduced length ΔL to length L_2, and it can be varied by simply varying L_1 while fixing L_2. The values of radiation rate γ as a function of the asymmetry parameter α for the dielectric metasurface are summarized in Fig. 3(b). It can be seen clearly that a quadratic dependence of γ on α is consistent with the theoretical relation in Eq. (10) for asymmetric resonances governed by BIC, i.e., $\gamma \propto \alpha^2$. Constrained with the general theory for the absorption bandwidth in Eq. (11), the reducing value of α as length L_1 increases to L_2 accounts for the narrowing bandwidth, which lays the foundation for FWHM manipulation dependent on the asymmetry parameter.

To construct a critical coupling system, a monolayer graphene is taken into account as a lossy component on top of the silicon nanobars. In hybrid metasurfaces, the inserted graphene determines the dissipative loss rate δ, while the radiation rate γ is dependent on the asymmetry degree of nanobars as above. When these two parameters are equal in the system, i.e., $\gamma = \delta$, the critical coupling condition is satisfied, and a maximum absorption is achieved. Figure 4(a) illustrates the absorption spectra for undoped graphene with respect to nanobar length L_1 and incident wavelength. The critical coupling point can be found by sweeping these two variables, and the maximum absorption of 0.5 is attained at 1427.39 nm with nanobar length $L_1 = 625$ nm. The simulated result is further verified by the fitting curve from Eq. (4), as shown in Fig. 4(b). The values of

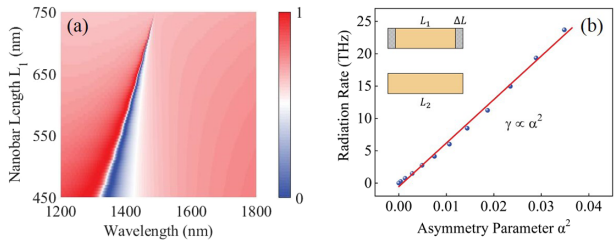

Fig. 3. (a) Transmission spectra of the dielectric metasurfaces as a function of the length L_1 of the shorter nanobar. (b) Values of radiation rate γ as a function of the asymmetry parameter α. Inset: the asymmetry parameter α is defined as $\Delta L/L_2$, where ΔL is half the difference between nanobar lengths L_1 and L_2.

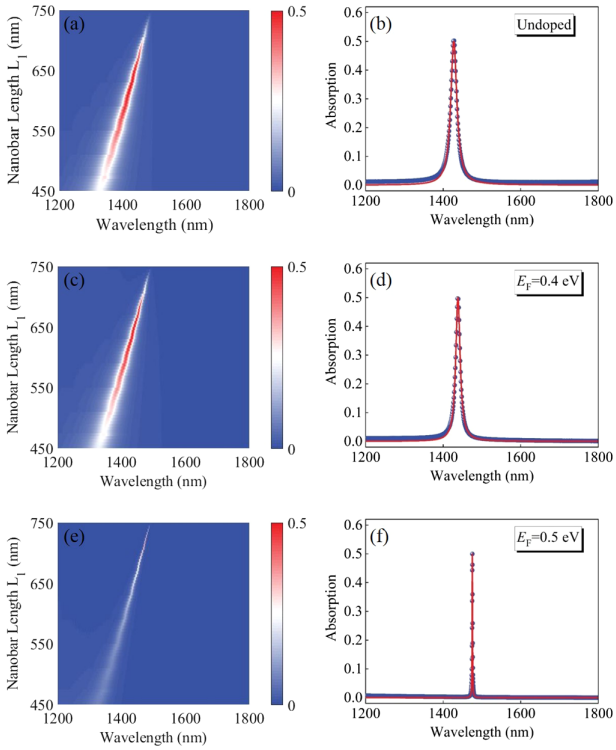

Fig. 4. (a), (c), (e) Absorption spectra of the hybrid graphene–dielectric metasurfaces as a function of the length L_1 of the shorter nanobar. (b), (d), (f) Simulated and fitted absorption spectra for graphene at critical coupling.

the radiation rate and dissipative loss rate can be extracted as $\gamma = \delta = 4.41$ THz, and the corresponding absorption bandwidth is $\Gamma^{\mathrm{FWHM}} = 19.06$ nm, showing a good match with the theoretical expression in Eq. (6).

Next we consider the absorption bandwidth at critical coupling when the monolayer graphene becomes doped. Based on the fact that the radiation rate γ and dissipative loss rate δ play crucial roles in determining the absorption characteristics, we control these two parameters to realize such manipulation. More specifically, δ is changed by tuning graphene conductivity via shifting its Fermi level, while γ is varied by adjusting the structural asymmetry of dielectric metasurfaces. The absorption spectra for doped graphene with respect to nanobar length L_1 and incident wavelength are plotted in Figs. 4(c) and 4(e), respectively. Here the Fermi levels of 0.4 and 0.5 eV are

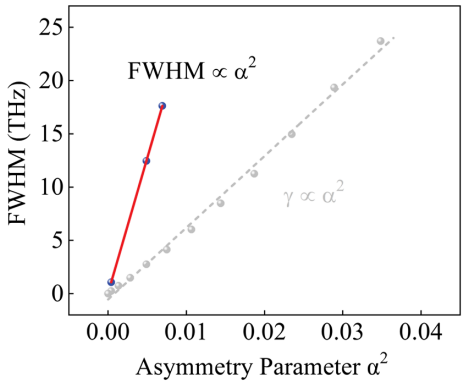

Fig. 5. Quadratic dependence of the absorption bandwidth FWHM (red line) and radiation rate γ (gray line) on the asymmetry parameter α.

adopted because the graphene conductivity exhibits a dramatic decrease across the Pauli-blocking point, which will remarkably reduce the dissipative loss. The critical coupling points can be found by sweeping nanobar length L_1 and incident wavelength, and the maximum absorption is attained at 1438.13 nm with $L_1 = 645$ nm for $E_F = 0.4$ eV and at 1475.26 nm with $L_1 = 720$ nm for $E_F = 0.5$ eV, respectively. The simulated results are once again verified by the fitting curves from Eq. (4), as shown in Figs. 4(d) and 4(f). Both spectra share an absorption peak of 0.5 in agreement with theoretical maximum. The values of the radiation rate and dissipative loss rate can be extracted as $\gamma = \delta = 3.11$ THz and $\gamma = \delta = 0.27$ THz, respectively. As a result of the simultaneous decreasing of γ and δ, the absorption bandwidth shrinks by more than one order of magnitude from 13.60 to 1.21 nm. As for the up-down symmetry, the dielectric metasurfaces have mirror symmetry in the out-of-plane direction. The graphene adds dissipative loss to the system, but it is so thin that it hardly breaks the up-down symmetry. Therefore, the derivation of Eqs. (1)–(11) is still valid. When the graphene is present, the BIC mode still manifests itself in the transmission spectrum as a Fano resonance as shown in Figs. S1(a), S1(b), and S1(c) of Supplement 1, and accordingly results in a symmetric Lorentzian line shape in the absorption spectrum as shown in Figs. 4(b), 4(d), and 4(f).

We further provide the dependence of absorption bandwidth FWHM on the asymmetry parameter α with different Fermi levels of graphene. Extracted from the critical coupling condition corresponding to cases of undoped graphene and doped graphene with 0.4 and 0.5 eV, respectively, the estimated FWHM is proportional to the square of α, as can be seen in Fig. 5, i.e., $\Gamma^{\mathrm{FWHM}} \propto \alpha^2$, and even more interesting, the slope of this linear fitting is four times that of the radiation rate in Fig. 3(b), which confirms the analytical description in Eq. (11). It is noted that the quadratic relation between radiation rate γ and asymmetric parameter α remains valid for the general case of asymmetry metasurfaces with high-quality resonance governed by BIC, and by parity of reasoning, the quadratic scalability of FWHM at critical coupling shows general applicability, offering a straightforward way to engineer the absorption properties.

4. CONCLUSION

In conclusion, we bridge a direct link between radiation control at critical coupling and intriguing BIC physics, and develop a generalized theory to engineer light absorption of 2D materials in coupling resonance systems. The quadratic dependence of the absorption bandwidth on the asymmetry parameter is obtained. In hybrid graphene–dielectric metasurfaces, the absorption bandwidth can be flexibly tuned by more than one order of magnitude by simultaneously adjusting the asymmetry parameter for silicon nanobar resonators and the graphene surface conductivity while the absorption efficiency remains maximum. Beyond this typical example, the proposed theoretical method should have wide applicability to diverse types of critical coupling systems, in principle, with various asymmetric metasurface designs and different atomically thin 2D materials throughout the spectrum. Therefore, this work not only gains a deeper physical insight into the enhanced light–matter interaction in 2D materials, but also paves a way towards smart design of compact optoelectronic devices such as light emitters, detectors, and modulators.

Funding. National Natural Science Foundation of China (11664024, 11847132, 11947065, 61901164); Natural Science Foundation of Jiangxi Province (20171ACB201020, 20202BAB211007); Interdisciplinary Innovation Fund of Nanchang University (2019-9166-27060003); China Scholarship Council (202008420045).

Acknowledgment. The authors thank Dr. S. Li for her guidance on the effective multipole expansion and Dr. X. Jiang for beneficial discussions on the critical coupling mechanism.

Disclosures. The authors declare no conflicts of interest.

Data Availability. Data underlying the results presented in this paper are not publicly available at this time but may be obtained from the authors upon reasonable request.

Supplemental document. See Supplement 1 for supporting content.

REFERENCES

1. F. Xia, H. Wang, D. Xiao, M. Dubey, and A. Ramasubramaniam, "Two-dimensional material nanophotonics," Nat. Photonics **8**, 899–907 (2014).
2. J. R. Piper and S. Fan, "Total absorption in a graphene monolayer in the optical regime by critical coupling with a photonic crystal guided resonance," ACS Photon. **1**, 347–353 (2014).
3. J. R. Piper, V. Liu, and S. Fan, "Total absorption by degenerate critical coupling," Appl. Phys. Lett. **104**, 251110 (2014).
4. H. Lu, B. P. Cumming, and M. Gu, "Highly efficient plasmonic enhancement of graphene absorption at telecommunication wavelengths," Opt. Lett. **40**, 3647–3650 (2015).
5. L. Huang, G. Li, A. Gurarslan, Y. Yu, R. Kirste, W. Guo, J. Zhao, R. Collazo, Z. Sitar, G. N. Parsons, M. Kudenov, and L. Cao, "Atomically thin MoS2 narrowband and broadband light superabsorbers," ACS Nano **10**, 7493–7499 (2016).
6. C.-C. Guo, Z.-H. Zhu, X.-D. Yuan, W.-M. Ye, K. Liu, J.-F. Zhang, W. Xu, and S.-Q. Qin, "Experimental demonstration of total absorption over 99% in the near infrared for monolayer-graphene-based subwavelength structures," Adv. Opt. Mater. **4**, 1955–1960 (2016).
7. J. Hu, Y. Qing, S. Yang, Y. Ren, X. Wu, W. Gao, and C. Wu, "Tailoring total absorption in a graphene monolayer covered subwavelength multilayer dielectric grating structure at near-infrared frequencies," J. Opt. Soc. Am. B **34**, 861–868 (2017).
8. X. Jiang, T. Wang, S. Xiao, X. Yan, and L. Cheng, "Tunable ultra-high-efficiency light absorption of monolayer graphene using critical coupling with guided resonance," Opt. Express **25**, 27028–27036 (2017).

9. H. Li, M. Qin, L. Wang, X. Zhai, R. Ren, and J. Hu, "Total absorption of light in monolayer transition-metal dichalcogenides by critical coupling," Opt. Express **25**, 31612–31621 (2017).
10. C. Zhou, G. Liu, G. Ban, S. Li, Q. Huang, J. Xia, Y. Wang, and M. Zhan, "Tunable Fano resonator using multilayer graphene in the near-infrared region," Appl. Phys. Lett. **112**, 101904 (2018).
11. X. Jiang, T. Wang, S. Xiao, X. Yan, L. Cheng, and Q. Zhong, "Approaching perfect absorption of monolayer molybdenum disulfide at visible wavelengths using critical coupling," Nanotechnology **29**, 335205 (2018).
12. H.-J. Li, Y.-Z. Ren, J.-G. Hu, M. Qin, and L.-L. Wang, "Wavelength-selective wide-angle light absorption enhancement in monolayers of transition-metal dichalcogenides," J. Lightwave Technol. **36**, 3236–3241 (2018).
13. Y. M. Qing, H. F. Ma, and T. J. Cui, "Tailoring anisotropic perfect absorption in monolayer black phosphorus by critical coupling at terahertz frequencies," Opt. Express **26**, 32442–32450 (2018).
14. A. Akhavan, S. Abdolhosseini, H. Ghafoorifard, and H. Habibiyan, "Narrow band total absorber at near-infrared wavelengths using monolayer graphene and sub-wavelength grating based on critical coupling," J. Lightwave Technol. **36**, 5593–5599 (2018).
15. S. Xiao, T. Liu, L. Cheng, C. Zhou, X. Jiang, Z. Li, and C. Xu, "Tunable anisotropic absorption in hyperbolic metamaterials based on black phosphorous/dielectric multilayer structures," J. Lightwave Technol. **37**, 3290–3297 (2019).
16. J. Wang, A. Chen, Y. Zhang, J. Zeng, Y. Zhang, X. Liu, L. Shi, and J. Zi, "Manipulating bandwidth of light absorption at critical coupling: an example of graphene integrated with dielectric photonic structure," Phys. Rev. B **100**, 075407 (2019).
17. T. Liu, X. Jiang, C. Zhou, and S. Xiao, "Black phosphorus-based anisotropic absorption structure in the mid-infrared," Opt. Express **27**, 27618–27627 (2019).
18. T. Liu, X. Jiang, H. Wang, Y. Liu, C. Zhou, and S. Xiao, "Tunable anisotropic absorption in monolayer black phosphorus using critical coupling," Appl. Phys. Express **13**, 012010 (2020).
19. S. Xiao, T. Liu, X. Wang, X. Liu, and C. Zhou, "Tailoring the absorption bandwidth of graphene at critical coupling," Phys. Rev. B **102**, 085410 (2020).
20. J. Wang, J. Yang, and D. Shi, "Perfect absorption for monolayer transition-metal dichalcogenides by critical coupling," Nanotechnology **31**, 465205 (2020).
21. Y. Cai, Y. Guo, Y. Zhou, X. Huang, G. Yang, and J. Zhu, "Tunable dual-band terahertz absorber with all-dielectric configuration based on graphene," Opt. Express **28**, 31524–31534 (2020).
22. C. W. Hsu, B. Zhen, J. Lee, S.-L. Chua, S. G. Johnson, J. D. Joannopoulos, and M. Soljačić, "Observation of trapped light within the radiation continuum," Nature **499**, 188–191 (2013).
23. F. Wu, J. Wu, Z. Guo, H. Jiang, Y. Sun, Y. Li, J. Ren, and H. Chen, "Giant enhancement of the Goos-Hanchen shift assisted by quasi-bound states in the continuum," Phys. Rev. Appl. **12**, 014028 (2019).
24. S. Romano, M. Mangini, E. Penzo, S. Cabrini, A. C. D. Luca, I. Rendina, V. Mocella, and G. Zito, "Ultrasensitive surface refractive index imaging based on quasi-bound states in the continuum," ACS Nano **14**, 15417–15427 (2020).
25. J. Zhang, K. F. MacDonald, and N. I. Zheludev, "Near-infrared trapped mode magnetic resonance in an all-dielectric metamaterial," Opt. Express **21**, 26721–26728 (2013).
26. A. Sayanskiy, A. S. Kupriianov, S. Xu, P. Kapitanova, V. Dmitriev, V. V. Khardikov, and V. R. Tuz, "Controlling high-q trapped modes in polarization-insensitive all-dielectric metasurfaces," Phys. Rev. B **99**, 085306 (2019).
27. K. Koshelev, Y. Tang, K. Li, D.-Y. Choi, G. Li, and Y. Kivshar, "Nonlinear metasurfaces governed by bound states in the continuum," ACS Photon. **6**, 1639–1644 (2019).
28. J. Tian, Q. Li, P. A. Belov, R. K. Sinha, W. Qian, and M. Qiu, "High-Q all-dielectric metasurface: super and suppressed optical absorption," ACS Photon. **7**, 1436–1443 (2020).
29. N. Bernhardt, K. Koshelev, S. J. White, K. W. C. Meng, J. E. Fröch, S. Kim, T. T. Tran, D.-Y. Choi, Y. Kivshar, and A. S. Solntsev, "Quasi-BIC resonant enhancement of second-harmonic generation in WS2 monolayers," Nano Lett. **20**, 5309–5314 (2020).
30. Y. Liang, K. Koshelev, F. Zhang, H. Lin, S. Lin, J. Wu, B. Jia, and Y. Kivshar, "Bound states in the continuum in anisotropic plasmonic metasurfaces," Nano Lett. **20**, 6351–6356 (2020).
31. V. R. Tuz, V. V. Khardikov, and Y. S. Kivshar, "All-dielectric resonant metasurfaces with a strong toroidal response," ACS Photon. **5**, 1871–1876 (2018).
32. Y. Fan, F. Zhang, N.-H. Shen, Q. Fu, Z. Wei, H. Li, and C. M. Soukoulis, "Achieving a high-Q response in metamaterials by manipulating the toroidal excitations," Phys. Rev. A **97**, 033816 (2018).
33. Y. He, G. Guo, T. Feng, Y. Xu, and A. E. Miroshnichenko, "Toroidal dipole bound states in the continuum," Phys. Rev. B **98**, 161112 (2018).
34. A. E. Miroshnichenko, A. B. Evlyukhin, Y. F. Yu, R. M. Bakker, A. Chipouline, A. I. Kuznetsov, B. Luk'yanchuk, B. N. Chichkov, and Y. S. Kivshar, "Nonradiating anapole modes in dielectric nanoparticles," Nat. Commun. **6**, 8069 (2015).
35. Y. Yang, V. A. Zenin, and S. I. Bozhevolnyi, "Anapole-assisted strong field enhancement in individual all-dielectric nanostructures," ACS Photon. **5**, 1960–1966 (2018).
36. Y. Yang and S. I. Bozhevolnyi, "Nonradiating anapole states in nanophotonics: from fundamentals to applications," Nanotechnology **30**, 204001 (2019).
37. C. Zhou, S. Li, M. Fan, X. Wang, Y. Xu, W. Xu, S. Xiao, M. Hu, and J. Liu, "Optical radiation manipulation of Si-Ge2Sb2Te5 hybrid metasurfaces," Opt. Express **28**, 9690–9701 (2020).
38. A. Kodigala, T. Lepetit, Q. Gu, B. Bahari, Y. Fainman, and B. Kanté, "Lasing action from photonic bound states in continuum," Nature **541**, 196–199 (2017).
39. M. V. Rybin, K. L. Koshelev, Z. F. Sadrieva, K. B. Samusev, A. A. Bogdanov, M. F. Limonov, and Y. S. Kivshar, "High-Q supercavity modes in subwavelength dielectric resonators," Phys. Rev. Lett. **119**, 243901 (2017).
40. H. A. Haus, *Waves and Fields in Optoelectronics* (Prentice-Hall, 1984).
41. S. Fan, W. Suh, and J. D. Joannopoulos, "Temporal coupled-mode theory for the Fano resonance in optical resonators," J. Opt. Soc. Am. A **20**, 569–572 (2003).
42. K. Koshelev, S. Lepeshov, M. Liu, A. Bogdanov, and Y. Kivshar, "Asymmetric metasurfaces with high-Q resonances governed by bound states in the continuum," Phys. Rev. Lett. **121**, 193903 (2018).
43. S. Li, C. Zhou, T. Liu, and S. Xiao, "Symmetry-protected bound states in the continuum supported by all-dielectric metasurfaces," Phys. Rev. A **100**, 063803 (2019).
44. J. Zhang, Z. Zhu, W. Liu, X. Yuan, and S. Qin, "Towards photodetection with high efficiency and tunable spectral selectivity: graphene plasmonics for light trapping and absorption engineering," Nanoscale **7**, 13530–13536 (2015).
45. S. Xiao, T. Wang, Y. Liu, C. Xu, X. Han, and X. Yan, "Tunable light trapping and absorption enhancement with graphene ring arrays," Phys. Chem. Chem. Phys. **18**, 26661–26669 (2016).
46. https://www.lumerical.com.